Characterization of pinning and vortex motion in thin superconducting microbridges

M. Pannetier, Ph. Lecoeur,* and P. Bernstein*
LUSAC-EIC (E. A. 2607), Site Universitaire de Cherbourg, F50130 Octeville, France

T. D. Doan and J. F. Hamet
CRISMAT-ISMRA (UMR-CNRS 6508), F14050 Caen, France
(Received 1 March 2000; revised manuscript received 17 July 2000)

We show that transport measurements carried out with and without a low applied magnetic field enable one to characterize the vortex dynamics in high-T_c superconducting films. The application of a low magnetic field induces a modulation of the critical current that depends on the process involved when the vortices are set in motion. Current-voltage measurements with no applied field yield information on the pinning energy, the pinning sites density, and the way the vortices are moving. Measurements carried out on a set of $YBa_2Cu_3O_7$ microbridges show that the vortex dynamics depend primarily on the pinning sites density. This quantity proves to be strongly dependent on the thickness of the superconducting film.

I. INTRODUCTION

The most popular parameters used to characterize the physics of the vortices in high-T_c superconducting films are the pinning energy and the pinning constant (or Labusch parameter). The determination of the pinning energy has been essentially carried out with three different techniques: measurement of the resistivity as a function of the applied magnetic field in the thermally activated flux flow (TAFF) regime,[1–4] ac magnetic susceptibility measurements,[5–7] and measurements of the current-voltage characteristics.[8–10] However, these techniques yield results that can be very different for the same type of sample, which means that they do not address the same physical phenomenon. The large pinning energy measured in the TAFF regime is probably linked to plastic deformations in the vortex lattice,[6,11] while the smaller quantity determined from the current-voltage characteristics and the susceptibility measurements most likely characterizes the pinning of individual vortices.[10] The determination of the pinning constant has been extensively investigated for different types of superconducting materials, notably the bismuth phases and $YBa_2Cu_3O_7$ (YBCO). Ceramics, thick films, thin films, and single crystals were investigated with various measurement methods such as a vibrating reed technique,[12] surface impedance measurements,[13,14] or inductive methods.[15] Transport measurements under high magnetic fields on YBCO films have also been used to determine the Labusch parameter from the force-displacement response.[16,17] In contrast to the results on the pinning energy, all these techniques have generally yielded similar results for the same material.

In this paper we show that important additional information on the individual pinning and the motion of the vortices can be obtained from transport measurements carried out on microbridges with and without an applied field. Section II deals with the modulation of the critical current by a low magnetic field. This field induces a screening current and creates a vortex lattice in the microbridge that cause the critical current modulation. We show that the measurement of this quantity enables one to get pertinent information on the process that sets the vortices in motion. Furthermore, we can determine the penetration depth and, in some cases, the superconducting thickness of the microbridge. This last quantity can be different from the physically deposited thickness because of interface effects or if corrosive agents have degraded the film. In Sec. III we propose a model for the current-voltage characteristics of the microbridges measured with no applied field in the flux creep regime. As a distinctive feature this model assumes that the motion of the vortices is due to a diffusion process. Then, we determine the pinning energy and the jump width of the vortices as well as the transition current from the flux creep to the flux flow regime. Furthermore, we determine the Labusch parameter in the temperature range in which the vortex motion occurs as that of straight vortices. The measurements described in Secs. II and III were carried out on a set of $YBa_2Cu_3O_7$ microbridges. The results are reported in Sec. IV and discussed in Sec. V.

II. MODULATION OF THE CRITICAL CURRENT BY A MAGNETIC FIELD

Let us consider a superconducting thin-film microbridge with length L, width w, deposited thickness d, superconducting thickness d^*, and a uniform magnetic field **B** applied perpendicular to the microbridge plane (see Fig. 1). According to magneto-optical observations of the flux penetration in superconducting thin-film disks, squares, or strips,[18,19] and Hall probe measurements,[19–21] if the flux penetration is incomplete, the flux enters the peripheral part of the sample

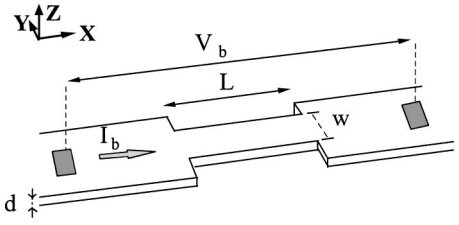

FIG. 1. Schema of a microbridge.

 ©2000 The American Physical Society

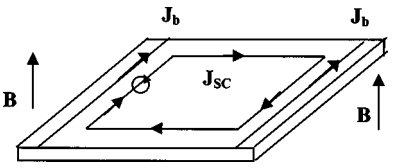

FIG. 2. Schema of the bias ($\mathbf{J}_b$) and screening current ($\mathbf{J}_{sc}$) lines, when magnetic field **B** is applied with no vortex lattice in the microbridge but with a vortex pinned along the nucleating edge.

only, while the central region is shielded by the screening current. If the bias current flows in the sample, a nonzero voltage is measured at the terminals of the microbridge when the vortex lattice is set in motion. This requires that vortices run across the area previously free of vortices. It is reasonable to assume that these vortices enter this area either by vortex nucleation or by vortex depinning. Then, the critical current is equal to the bias current amplitude required for the relevant process. In this section, we estimate the critical current modulation, $\Delta I_{cr}(B)$, for both processes.

A. Contribution of the screening current

Let us suppose that field **B** is applied with no vortex in the superconductor. Then, a screening current with current density J_{sc} flows in the sample (see Fig. 2). From the London relation, along the edges of the microbridge we have (see Fig. 1 for the axes orientation)

$$B=\mu_0\lambda^2\frac{\partial J_{sc}}{\partial y} \quad \text{with} \quad \frac{\partial J_{sc}}{\partial y}\approx\frac{J_{sc}^0}{\lambda} \tag{1a}$$

and

$$B_{sf}=\mu_0\lambda^2\frac{\partial J_b}{\partial y}, \quad \text{with} \quad \left|\frac{\partial J_b}{\partial y}\right|\approx\frac{J_b^0}{\lambda}. \tag{1b}$$

In Eqs. (1a) and (1b), λ is the penetration depth in the microbridge plane, J_{sc}^0 and J_b^0 are the absolute values of the local screening and bias current density, respectively, and B_{sf} is the z component of the bias current self-field. From Eqs. (1a) and (1b), the following equations can be derived:

$$B=\mu_0\lambda J_{sc}^{(0)} \tag{2a}$$

and

$$|B_{sf}|=\mu_0\lambda J_b^0. \tag{2b}$$

1. Vortex nucleation

Let us consider the edge along which the bias and screening current densities add up (see Fig. 2). Vortex nucleation takes place when the total field along this edge is equal to a threshold value. The magnitude of the threshold depends on the type of barrier impeding the entry of the vortices[22–26] and, as pointed out by Likharev[27] and Aranson, Gitterman, and Shapiro,[28] the entry of the vortices is not necessarily coherent. However, in any case, the vortex nucleation condition can be written as

$$B_{cr0}=B_{cr1}+B, \tag{3}$$

where B_{cr0} and B_{cr1} are the nucleation self-fields for $B=0$ and $B\neq 0$, respectively. From Eqs. (2a) and (2b), Eq. (3) takes the form

$$J_{cr0}^0=J_{cr1}^0+J_{sc}^0, \tag{4}$$

where J_{cr0}^0 and J_{cr1}^0 are the critical current densities along the nucleating edge for $B=0$ and $B\neq 0$, respectively. ΔI_{cr1} is defined as the critical current modulation due to the screening current. This quantity is equal to the change in the bias current that would cause an increase in the bias current density equal to J_{sc}^0 along the nucleating edge. Let $\Delta J_b(y)$ be the corresponding bias current density change. We consider only thin films with $d\ll\lambda$, then we can write

$$\Delta I_{cr1}=d^*\int_{-w/2}^{w/2}\Delta J_b dy. \tag{5}$$

J_b and ΔJ_b are Meissner current densities since no vortex has entered the film. Furthermore, in the cases we deal with we have $w\gg\lambda$, then we assume that ΔJ_b can be written as

$$\Delta J_b=J_{sc}^0\left[e^{-[(w/2+y)/\lambda]}+e^{-[(w/2-y)/\lambda]}\right]$$

$$=2J_{sc}^0e^{-w/2\lambda}\cosh\left(\frac{y}{\lambda}\right). \tag{6}$$

From Eqs. (2a), (5), and (6), ΔI_{cr1} takes the form

$$\Delta I_{cr1}=I_{cr0}-I_{cr1}\approx 2J_{sc}^0d^*\lambda=\frac{2Bd^*}{\mu_0}, \tag{7}$$

where I_{cr0} and I_{cr1} are the critical current values without and with applied field, respectively.

2. Vortex depinning

Along the nucleating edge of the microbridge, according to the same reasoning as in the case of the nucleation process, the vortex depinning condition can be written as

$$F_{cr0}=F_{cr1}+F_{sc}, \tag{8}$$

where F_{cr0} and F_{cr1} are the Lorentz forces due to the bias current for $B=0$ and $B\neq 0$, respectively, and F_{sc} is the Lorentz force due to the screening current. Equation (8) takes the form

$$J_{cr0}^0\phi_0=J_{cr1}^0\phi_0+J_{sc}^0\phi_0, \tag{9}$$

where ϕ_0 is the flux quantum. Equation (9) is equivalent to Eq. (4). Then, Eq. (7) gives the critical current modulation. An identical result was obtained from the vortex diffusion model in Ref. 9. We observe that it is not possible, according to these results, to discriminate the nucleation process from the depinning process. However, the model is not complete, since it does not account for the effect of the vortex lattice that has possibly entered the microbridge.

B. Contribution of the vortex lattice and determination of $\Delta I_{cr}(B)$

When vortices have entered the sample, the screening current does not collapse but flows around the area free of vortices[22,23] (see Fig. 3). As a consequence, we shall assume

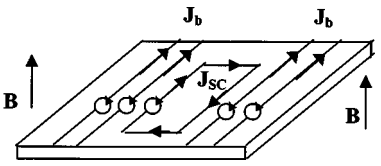

FIG. 3. Schema of the bias ($\mathbf{J}_b$) and screening current ($\mathbf{J}_{sc}$) lines, when the vortex lattice has entered part of the microbridge.

in what follows that ΔI_{cr1} accounts for the effect of the screening current upon the total critical current modulation.

1. Vortex nucleation

By analogy with the previous section we assume that a vortex is nucleated in the area free of vortices if the total field along the border with the area entered by the vortices is equal to a threshold value. This condition can be written as

$$B_{cr1}=B_{cr}+B_v\,. \tag{10}$$

In Eq. (10), B_{cr} is the nucleation self-field and B_v is the field due to the vortex lattice. For the sake of simplicity, we will assume a square array for the vortex lattice with a period

$$a=\sqrt{\phi_0/B}. \tag{11}$$

The nucleated vortex is most probably located at the end of a vortex row. B_v can be written as[29]

$$B_v=\frac{\phi_0}{2\pi\lambda^2}\sum_k K_0\left(\frac{r_k}{\lambda}\right). \tag{12}$$

In Eq. (12), K_0 is the modified Bessel function of zero order, r_k is the distance between vortex k and the nucleated vortex, and the sum is extended to all the vortices in the lattice. Then, using Eq. (2b), the nucleation condition [Eq. (10)] takes the form

$$\mu_0\lambda J_{cr1}=\mu_0\lambda J_{cr}+\frac{\phi_0}{2\pi\lambda^2}\sum_k K_0\left(\frac{r_k}{\lambda}\right), \tag{13}$$

where J_{cr} is the nucleation current density. Since in the area entered by the vortices the current distribution is assumed to be uniform,[22,30] we can write

$$J_{cr1}\approx\frac{I_{cr1}}{wd^*},$$

$$J_{cr}\approx\frac{I_{cr}}{wd^*}. \tag{14}$$

Then, the total critical current modulation takes the form

$$\Delta I_{cr}=I_{cr0}-I_{cr}=\frac{2d^*B}{\mu_0}+\frac{\phi_0 wd^*}{2\pi\mu_0\lambda^3}\sum_k K_0\left(\frac{r_k}{\lambda}\right), \tag{15}$$

where I_{cr} is the critical current when field B is applied.

2. Vortex depinning

A vortex located at the border of the area penetrated by the vortex lattice is pushed forward into the area free of vortices by the Lorentz forces due to the bias and screening currents and the force exerted by the other vortices. The depinning condition takes the form

$$F_{cr1}=F_{cr}+F_v\,, \tag{16}$$

where F_v is the force exerted by the other vortices and F_{cr} is the force due to the bias current. If we assume that the pinning sites are randomly distributed and that, because of thermal activation, the individual vortices can jump from one pinning site to the other one, then the lattice is not regular. As a result, F_v is probably due, for the most part, to the vortices of the same row. Furthermore, distance a in Eq. (11) is not the actual but the average distance between two vortices. Although a fluctuation in the distance between any pair of vortices in the row is possible, the contribution to F_v of the nearest neighbor is dominant. As a result, depinning is made easier if the actual distance between the vortex located at the border and this neighbor is equal to $(a-h)$, with $h\geqslant 0$. Then, instead of its classical expression (see Ref. 29), F_v can be written as

$$F_v=\frac{\phi_0^2}{2\pi\mu_0\lambda^3}\sum_k K_1\left(\frac{ka-h}{\lambda}\right). \tag{17}$$

In Eq. (17), K_1 is the modified Bessel function of first order and the sum is extended to all the vortices in the row. As a result, Eq. (16) takes the form

$$J_{cr1}=J_{cr}+\frac{\phi_0}{2\pi\mu_0\lambda^3}\sum_k K_1\left(\frac{ka-h}{\lambda}\right) \tag{18}$$

and, from Eqs. (14) and (18), the critical current modulation can be written as

$$\Delta I_{cr}=I_{cr0}-I_{cr}=\frac{2d^*B}{\mu_0}+\frac{\phi_0 wd^*}{2\pi\mu_0\lambda^3}\sum_k K_1\left(\frac{ka-h}{\lambda}\right). \tag{19}$$

We have obtained two different expressions for ΔI_{cr}, which depend on the process involved when the vortex lattice is set in motion. As a result, from $\Delta I_{cr}(B)$ measurements it is possible to determine which process is relevant.

III. CHARACTERIZATION OF THE VORTEX MOTION

A. Pinning energy and jump width

When vortices are in motion, the amplitude of the voltage, V_b, induced at the microbridge terminals, is written as

$$V_b=nLv_L\phi_0\,. \tag{20}$$

In Eq. (20), n is the surface vortex density and v_L is the vortex velocity. The vortices nucleated by the self-field show a concentration gradient in contrast to the uniform distribution generated by an externally applied uniform magnetic field. As a result, we assume that their motion is due to a diffusion process and describe it with a mean-field model.[9] Then, the vortex density due to the self-field along the edges of the microbridge can be determined. We obtain

$$n\left(\frac{w}{2}\right)=\frac{\mu_0[I_b-I_{cr0}]}{2\phi_0 d^*}\quad\text{for } I_b>I_{cr0}$$

and

TABLE I. Width (w), length (L), deposited YBCO thickness (d), and critical temperature (T_c) of the investigated microbridges. Microbridges $S1A$ and $S1B$ were patterned from the same sample but have dimensions different from each other.

Microbridge	w (μm)	L (μm)	d (nm)	T_c (K)
$S1A$	13	18.5	40 ± 5	88.8 ± 0.1
$S1B$	23	36	40 ± 5	88.7 ± 0.1
$S2$	13	18.5	20 ± 5	88.4 ± 0.1
$S3$	13	18.5	<20	83.7 ± 0.2
$S4$	13	18.5	10 ± 5	86 ± 0.1

$$n\left(\frac{w}{2}\right)=0 \quad \text{for } I_b \leqslant I_{cr0}. \tag{21}$$

In the flux creep regime, assuming that pinning is individual with a single pinning energy E_p, the vortex velocity can be written as[31]

$$v_L = 2\omega_0 \delta e^{-E_p/k_BT} \sinh\left(\frac{W}{k_BT}\right). \tag{22}$$

In Eq. (22), ω_0 is the thermal activation attempt frequency, δ is the jump width, and W is the work carried out by the Lorentz force when a vortex is extracted from a pinning site. Since we consider individual vortices, we use the Heisenberg relation to estimate ω_0 ($\omega_0 \approx 10^{13}\,\mathrm{s}^{-1}$). W can be written as

$$W = J_b d^* \delta\phi_0 \approx \frac{I_b}{w}\delta\phi_0. \tag{23}$$

V_b takes the form

$$V_b = \left[\frac{\mu_0 L \omega_0 \delta \exp(-E_p/k_BT)}{d^*}\right][I_b - I_{cr0}] \times \sinh\left[\frac{I_b}{\left(\frac{wk_BT}{\delta\phi_0}\right)}\right] \quad \text{for } I_b > I_{cr0}$$

and

$$V_b = 0 \quad \text{for } I_b \leqslant I_{cr0}. \tag{24}$$

As a result, at each temperature, E_p and δ can be determined by fitting the measured current-voltage characteristics with Eq. (24).

B. Transition current from the flux creep to the flux flow regime and Labusch parameter

Transition from the flux creep to the flux flow regime occurs when the Lorentz force $\mathbf{F}_L$, due to the bias current, is equal to the maximum value of the pinning energy gradient.[32] According to Brandt,[33,34] E_P is an elastic energy, and the jump width is either the vortex spacing, or the separation of the pins, or the pinning range. We assume that the vortices jump from one pinning site to another and that the pinning range is the same as the separation of the pinning sites. Then, δ is a measurement of the pinning sites density. We can write

$$F_L = J_T \phi_0 d^* = 2\frac{E_p}{\delta}, \tag{25}$$

where J_T is the transition current density. As a result, the transition current I_T is written as

$$I_T \approx \frac{2E_p w}{\delta\phi_0}. \tag{26}$$

Furthermore, if the vortex motion can be described as that of straight vortices, the pinning energy takes the form

$$E_P = \tfrac{1}{2}\,\alpha_L d^* \delta^2, \tag{27}$$

and the Labusch parameter α_L can be computed from E_P and δ.

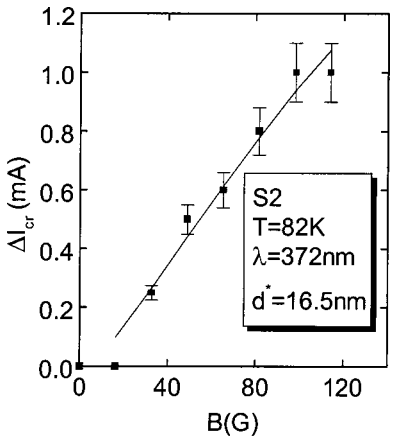

FIG. 4. Plot of the experimental critical current modulation $\Delta I_{cr}(B)$ measured on microbridge $S2$ at $T=82$ K (full squares) and best fit obtained with Eq. (15) (solid line). The inset shows the value of the fitting parameters, d^* and λ (superconducting thickness and superconducting penetration depth, respectively).

IV. EXPERIMENTAL RESULTS

A. Samples

We report measurements carried out on thin-film microbridges. The superconducting layers of the samples were c-axis-oriented YBCO films deposited by laser ablation on an $LaAlO_3$ substrate. Each sample was capped with a 20-nm-thick $La_4BaCu_5O_{13}$ overlayer and a gold layer to facilitate

TABLE II. Superconducting thickness (d^*) and penetration depth (λ) obtained for microbridge $S2$ from the best fits of $\Delta I_{cr}(B)$ with Eq. (15).

T (K)	75	77	80	82	84	86	87
d^* (nm)	20 ± 7	13.8 ± 1.9	34 ± 18	16.5 ± 2.4	20 ± 6	20 ± 25	14 ± 25
λ (nm)	363 ± 170	254 ± 105	634 ± 372	372 ± 76	544 ± 168	842 ± 1340	924 ± 2200

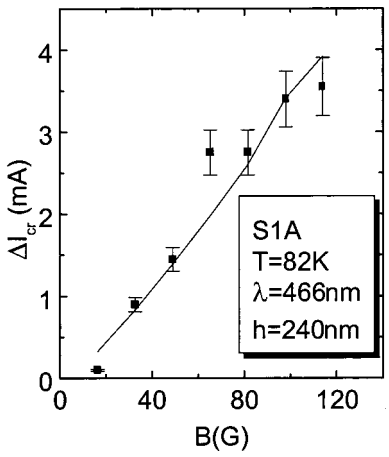

FIG. 5. Plot of the experimental critical current modulation $\Delta I_{cr}(B)$ measured on microbridge $S1A$ at $T=82$ K (full squares) and best fit obtained with Eq. (19) (solid line). The inset shows the value of the fitting parameters λ and h (superconducting penetration depth and fluctuation in the distance between the vortex entering the vortex free area and its nearest neighbor, respectively).

contact. $La_4BaCu_5O_{13}$ is a conductive oxide the properties of which were described elsewhere.[35] The gold layer was thin enough to have no sensible effect on the measurements. The samples were patterned as microbridges by conventional photolithography and chemical etching. The dimensions, thickness, and critical temperature of the microbridges are reported in Table I. We point out that since the critical current increases dramatically as temperature decreases, the measurements could be carried out in a limited range of temperature below T_c only.

B. Measurements of the critical current modulation

1. Measurements and fitting procedures

We have measured $\Delta I_{cr}(B)$ as a function of temperature on microbridges $S1A$, $S1B$, $S2$, and $S3$. At a given temperature, the measurements were performed for eight values of the applied field ranging from 0 to 114 G. Then, for each value of the magnetic field, the critical current was estimated with the 1-μV criterion, and $\Delta I_{cr}(B)$ was determined. Contrary to the results reported by Gaevski *et al.*,[30] who could trace a dependence of J_{cr} vs B only above $B\approx 200$ G when measuring YBCO strips, the obtained $\Delta I_{cr}(B)$ values were not negligible as compared to I_{cro} at the same temperature. The $\Delta I_{cr}(B)$ values were fitted with Eqs. (15) and (19). Only the terms corresponding to the three vortices in the lattice nearest the nucleation site were included in the sum of Eq. (15), and only those corresponding to the two first vortices in the row were included in the sum of Eq. (19). As usual, each fitting session was initialized by setting the fitting parameters in the range of the expected values. The fitting parameters were d^* and λ when the fitting procedure was carried out with Eq. (15). Then, a good fit could be obtained easily in most cases, as shown in Fig. 4. Table II shows the value of the fitting parameters obtained for $S2$ as a function of temperature. We observe that the determination of the fitting parameters lacks accuracy at high temperature. This is also true for the other microbridges.

In order to obtain unequivocal results, one of the three parameters (d^*, λ, or h) was fixed when fitting with Eq. (19). In the case of $S1A$, $S1B$, and $S2$, d^* was set equal to d. Consequently, the superconducting thickness of these microbridges could not be obtained from this fitting procedure. In the case of microbridge $S3$, since in the whole temperature range of the measurements the current-voltage characteristics are typical of the flux flow regime (see below), h was set equal to zero and a value could be determined for d^*. Again, in most cases, a good fit could be obtained easily (see Fig. 5 for an example). As a general rule, λ is determined with a better accuracy when fitting with Eq. (19) than when fitting with Eq. (15) (for an example, compare the results in Table II with those in Table III).

TABLE IV. Deposited thickness (d) and superconducting thickness (d^*) of the investigated microbridges obtained with the fitting procedures using either Eq. (15) or Eq. (19). The d^* values are averaged over the temperature range of the measurements.

Microbridge	d (nm)	d^* (nm) Eq. (15)	d^* (nm) Eq. (19)
$S1A$	40	74±13	
$S1B$	40	189±100	
$S2$	20	20±7	
$S3$	<20	6.5±1.4	6.3±1.5

2. Results

Table IV shows the superconducting thickness of the investigated microbridges obtained using Eq. (15) for $S1A$, $S1B$, and $S2$, and using, in turn, Eqs. (15) and (19) for $S3$.

The d^* values obtained for $S1A$ and $S1B$ with the fitting procedure using Eq. (15) show a large discrepancy with the value of the deposited thickness. On the contrary, the d^* value obtained for $S2$ is very near the deposited thickness. For $S3$, Eqs. (15) and (19) yield a quasi-identical d^* value that lies in the expected range of magnitude. In summary, the vortex nucleation model does not bring consistent results in the case of $S1A$ and $S1B$. Then, it is not possible to estimate the superconducting thickness of these microbridges. However, the nucleation model brings consistent d^* values for

TABLE III. Penetration depth (λ) and fluctuation in the distance between the vortex entering the vortex free area and its nearest neighbor (h) obtained for microbridge $S2$ from the best fits of $\Delta I_{cr}(B)$ with Eq. (19) (no reliable fitting parameters could be obtained at $T=77$ K).

T (K)	75	77	80	82	84	86	87
λ (nm)	461±9		538±3	551±11	524±6	820±80	2117±553
h (nm)	158±40		198±27	98±12	60±25	0	0

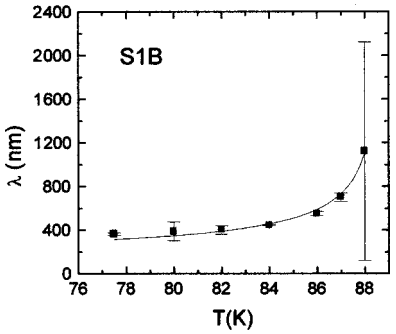

FIG. 6. Penetration depth $\lambda(T)$ computed for sample $S1B$ with the fitting procedure using Eq. (19). The solid line is a fit of these values using the two-fluid model.

$S2$, as do the nucleation and the depinning models for $S3$.

The $\lambda(T)$ values obtained for $S1B$ using Eq. (19) (assuming $d=d^*$) and those obtained for $S2$ with both fitting procedures are plotted in Figs. 6 and 7, respectively. Since the YBCO layer of our samples is c-axis oriented, λ is the penetration depth in the (a, b) plane of the perovskite structure. In the case of $S2$ the $\lambda(T)$ values obtained using both fitting procedures lie in a close range and can be fitted using the two-fluid model. This is also the case of the values obtained for $S1B$ with Eq. (19). Microbridges $S1A$ and $S3$ behave as $S1B$ and $S2$, respectively. Table V shows $\lambda(0)$ as obtained using the two-fluid model and the $\lambda(T)$ values computed with Eq. (19) [and Eq. (15) in the case of $S2$].[36]

As expected both $\lambda(0)$ values computed for $S2$ lie in a close range. Otherwise, the values in Table V are very similar and are in the range of the values obtained by surface impedance measurements at microwave frequencies on thicker films.[37–39] The determination of d^* and $\lambda(T)$ shows that the nucleation model is relevant for $S2$ and $S3$ but not for $S1A$ and $S1B$. Furthermore, the depinning model proves relevant for all the microbridges. Then, it is possible to make a reliable estimation of $h(T)$.

The $h(T)$ values obtained from the fits with Eq. (19) are plotted in Fig. 8 for $S1A$, $S1B$, and $S2$ (assuming $d=d^*$ for $S1A$ and $S1B$). As a predictable result of thermal activation, h decreases as temperature increases and goes to zero in the vicinity of T_c. The current-voltage characteristics measured at zero applied field on $S1A$, $S1B$, and $S2$ in the temperature range where h is found equal to zero show a large linear

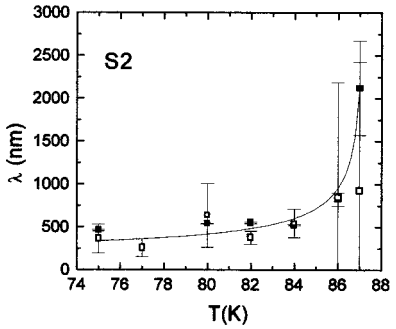

FIG. 7. Penetration depth $\lambda(T)$ computed for sample $S2$ with the fitting procedures using Eq. (15) (open squares) and Eq. (19) (full squares). The solid line is a fit using the two-fluid model of the values obtained with Eq. (19).

TABLE V. Penetration depth at $T=0$ K [$\lambda(0)$] in microbridges $S1A$, $S1B$, and $S2$. $\lambda(0)$ is computed using the two-fluid model and the $\lambda(T)$ values obtained using either the nucleation model [Eq. (15)] or the depinning model [Eq. (19)].

Microbridge	$S1A$ Eq. (19)	$S1B$ Eq. (19)	$S2$ Eq. (19)	$S2$ Eq. (15)
$\lambda(0)$ (nm)	232 ± 25	202 ± 10	225 ± 22	251 ± 40

part as do those measured on $S3$. For the sake of comparison the current-voltage characteristics measured (i) on $S1B$ at 88 K ($h=0$), and 87 K ($h=86$ nm) and (ii) on $S3$ at 78 K are reported in Figs. 9(a)–9(c), respectively. Current-voltage curves with the same features as in Figs. 9(a) and 9(c) correspond to microbridges driven in the flux flow regime.[40] We observe that, at a sufficiently high temperature, all the microbridges can be driven in this regime.

C. Measurements without applied field

The current-voltage characteristics of microbridges $S1A$, $S2$, $S3$, and $S4$ were measured with no applied magnetic field according to the conventional four-point method using a 1-kHz alternating current. In the case of $S1A$ and $S4$, d^* was set equal to d.

1. Pinning energy

Figure 10 shows the pinning energy of the microbridges as a function of the reduced temperature, T/T_c. The E_p values for $S2$, $S3$, and $S4$ lie almost on the same curve and are larger than the values computed for $S1A$ at the same reduced temperature.

2. Jump width

Figure 11 shows the value of the jump width of the microbridges as a function of T/T_c. As a general rule, the thinner the sample, the larger the jump width. In particular, the δ values for $S3$ and $S4$ are more than one order of magnitude larger than for $S1A$. This suggests that, although the pinning energy of $S1A$ is lower than that of the other samples, pinning is much more effective in $S1A$ than it is in

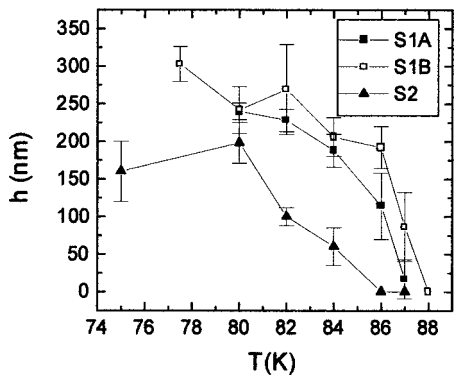

FIG. 8. Fluctuation $h(T)$ in the distance between the vortex entering the vortex free area and its nearest neighbor, determined for microbridges $S1A$, $S1B$, and $S2$ with the fitting procedure using Eq. (19). The solid lines are guides for the eye only.

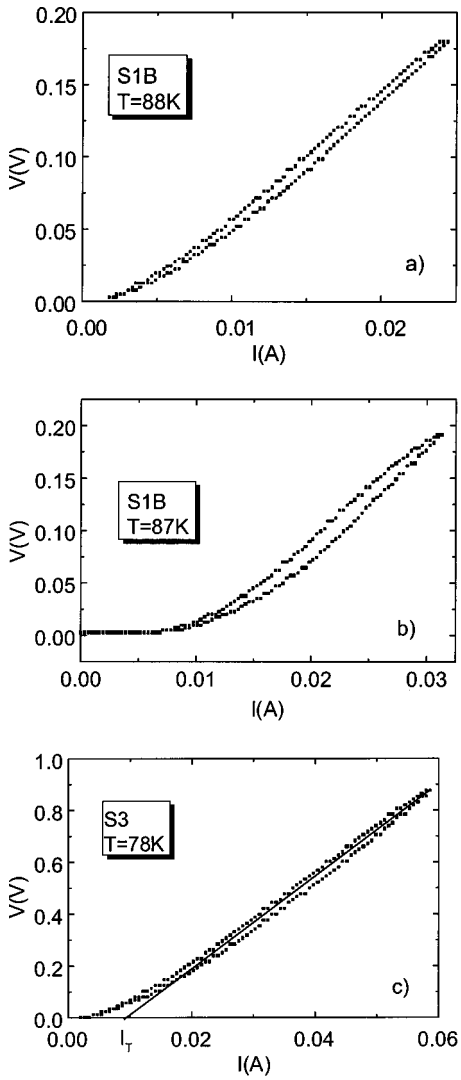

FIG. 9. Current-voltage characteristic at zero applied field measured on (a) microbridge $S1B$ at $T=88$ K, (b) microbridge $S1B$ at 87 K, and (c) microbridge $S3$ at $T=78$ K. The transition current (I_T) is measured at the intersection of the extrapolated flux flow branch with the current axis, as shown in (c).

the other microbridges. This is supported by the very narrow temperature range below T_c in which $S1A$ can be driven in the flux flow regime with no thermal runaway (see Table VI).

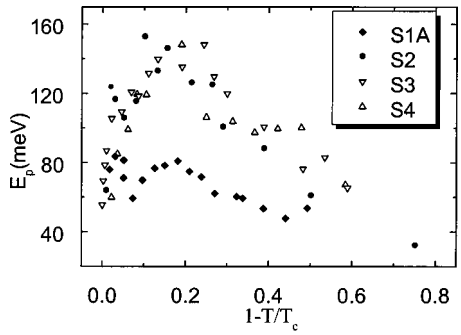

FIG. 10. Pinning energy (E_p) of the investigated microbridges as a function of the reduced temperature (T/T_c).

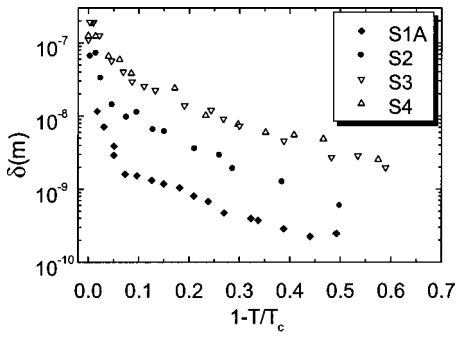

FIG. 11. Jump width (δ) of the investigated microbridges as a function of the reduced temperature (T/T_c).

3. Labusch parameter

The α_L values computed for the investigated microbridges according to Eq. (27) and the values obtained from surface impedance measurements on a large number of YBCO films by Golosovsky *et al.*[14] are reported in Fig. 12. We observe a strong disagreement between some of our results and the values of Golosovsky *et al.* We have reported in Fig. 12 two vertical lines, the solid line for $S3$ and $S4$ and the dashed line for $S2$. In each case, the line divides the figure in two zones where $\delta>2d$ and $\delta<2d$, respectively. In the case of $S3$ and $S4$, the agreement between the computed and the values of Golosovsky *et al.* is good in the zone where $\delta>2d$ and bad in the other zone. In the case of $S2$, the zone where $\delta>2d$ is very narrow. However, in this zone, we observe that the values computed for $S2$, $S3$, and $S4$ lie in a close range and are consistent with the values of Golosovsky *et al.* at a lower temperature. In the case of $S1A$, there is no temperature range where $\delta>2d$, and, at any temperature, the computed α_L values are much larger than the values of Golosovsky *et al.*

4. Transition current from the flux creep to the flux flow regime

In the flux flow regime, V_b takes the form

$$V_b=R_D(I_b-I_T), \tag{28}$$

where R_D is the dynamic resistance of the microbridge. As a result, the experimental value of the transition current can be determined from the linear part of the current-voltage characteristics [see Fig. 9(c)]. In Fig. 13, the experimental I_T values measured on $S2$, $S3$, and $S4$ are compared to the values obtained with Eq. (26) ($S1A$ can be driven in the flux flow regime in a temperature range too narrow to give meaningful results). A good agreement between both values of I_T is found for all the samples in a large temperature range.

TABLE VI. Temperature range below T_c in which the current-voltage characteristics measured on the microbridges can be driven in the flux flow regime with no thermal runaway.

Microbridge	$S1A$	$S2$	$S3$	$S4$
ΔT_c (K)	2.5	6.5	21	15

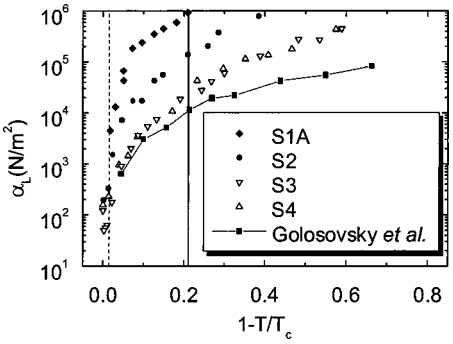

FIG. 12. Plot of the Labusch parameter $[\alpha_L(T/T_c)]$ as computed for the investigated microbridges according to Eq. (27) and as obtained from surface impedance measurements by Golosovsky *et al.* (Ref. 14). The solid line (the dash line) shows the separation for $S3$ and $S4$ ($S2$) between the zones where $\delta<2d$ and $\delta>2d$.

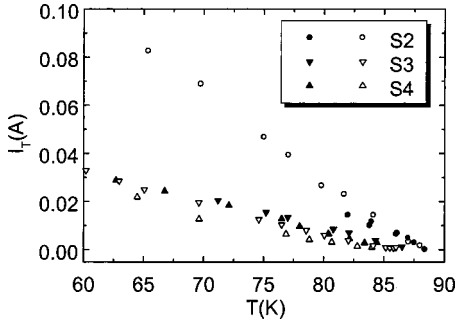

FIG. 13. Plot of the transition current from the flux creep to the flux flow regime $[I_T(T)]$ for the investigated microbridges. The solid symbols are experimental results, and the open symbols show the values obtained with Eq. (26).

V. DISCUSSION

A. Demagnetizing effects

The model detailed in Sec. II does not take into account the effect of the demagnetizing field (see the Appendix). However, the values obtained for $\lambda(0)$ are in agreement with those determined by surface impedance measurements. Furthermore, the model has yielded consistent d^* values in the case of the thinnest microbridges ($S2$ and $S3$). The reason that the demagnetizing field can be discarded is not clear. However, we can remark that since a microbridge is a very small object included in a much larger superconducting assembly, its demagnetizing field factor is certainly different from that of the isolated and much wider rectangular strips generally investigated by other authors.[19,21,30,41]

B. Vortex pinning

The results obtained when measuring $\Delta I_{cr}(B)$ on $S1A$ and $S1B$ give identical conclusions. This shows that the width of the microbridges has no effect on vortex pinning at least for the microbridges whose width is in the 10-μm range. Otherwise, the vortex depinning model is relevant for all the microbridges. However, consistent results have also been obtained with the nucleation model in the case of $S2$ and $S3$. This suggests that nucleation competes with depinning in the case of the very thin microbridges because pinning is less important in these films than in thick films. From studies on $YBa_2Cu_3O_7/PrBa_2(Cu_{1-x}Ga_x)_3O_7$ superlattices[42,43] Contour and co-workers have shown that stress relaxation occurs during the growth of YBCO films above a critical thickness $d_c \approx 10$ nm. Then, it is reasonable to infer that there are much fewer pinning sites in films with $d \leqslant d_c$ than in thick films because most of the pinning defects (dislocations or twin boundaries) are generated by the stress relaxation. This conclusion is consistent with the large value of the jump width of the microbridges whose thickness is in the range of d_c ($S3$ and $S4$) with respect to that of the thicker samples ($S2$ and $S1A$).

C. Vortex motion

The α_L values computed for our samples are in a good agreement with the values of Golosovsky *et al.* in the temperature range in which the jump width is much larger than the thickness of the YBCO film. The disagreement between the computed values and the values of Golosovsky *et al.* outside this range can be attributed to the fact that the straight vortex description is valid only if the YBCO film is thinner than a characteristic length l_c. In the opposite case, vortex motion occurs either by deformation of the vortex lines, as described by the Larkin and Ovchinnikov model (LO model),[44,45] or according to Schalk *et al.*,[10] by the motion of pancake vortices. This inference is supported by the strong disagreement between the α_L values computed for $S1A$ and the values of Golosovsky *et al.* in the whole range of temperature. Brunner *et al.*,[3] from measurements on superlattices, have estimated that in YBCO films l_c lies in the 45-nm range in the near vicinity of T_c. According to both the LO model [see Eq. (29) below and Fig. 11] and the model of Schalk *et al.*, l_c is an increasing function of temperature. Then, the thickness of $S1A$ is larger than l_c in the whole temperature range. As a consequence, for this microbridge, Eq. (27) and the computed α_L are expected to be incorrect.

We have assumed that δ is closely related to the separation between pinning sites. Then, in the framework of the LO model, l_c depends on the jump width as

$$l_c = \frac{\delta}{\gamma}, \tag{29}$$

where γ is the anisotropy factor of the superconductor. As a result, according to the LO model the α_L values computed with Eq. (27) are valid only in the range of temperature where $\delta \gg d$. This proves correct for $S2$, $S3$, and $S4$. Now, the good agreement between the measured and computed I_T values in the case of these microbridges could look surprising, since Eq. (27) is valid in a much narrower temperature range. However, the only condition of validity of Eqs. (25) and (26) is that E_P is an elastic energy. The results in Fig. 13 show that it is the case, although the pinning energy does not take the form of Eq. (27) in the zones where $\delta \approx d$. From a general point of view our results show a qualitative agreement with the LO model. However, the commonly admitted value for the anisotropy factor is $\gamma \approx 5-6$ in the case of YBCO.[46] The results obtained with $S2$, $S3$, and $S4$ suggest that the thickness range in which the vortex motion is not dominated by the deformation process is somewhat larger than that inferred from Eq. (29). This could be due to the fact

that Eq. (29) was established for superconductors under a high applied magnetic field, which is not the case for our measurements.

In the model of Schalk *et al.* individual pancake vortices are displaced almost independently at low temperature while, with increasing temperature the number of pancake vortices that are displaced together, and as a result, the value of l_c, are increasing. At 77 K, l_c is found to lie in the 15–20-nm range in the case of YBCO, which is consistent with our results. However, the existence of pancake vortices in YBCO is still a controversial point.

VI. CONCLUSION

We have shown that the critical current modulation and current-voltage measurements with no applied field enable one to characterize the vortex dynamics in superconducting microbridges. In YBCO films both characterizations give results consistent with each other. In these films the relevant parameter to describe pinning is not the pinning energy but the jump width, i.e., the pinning sites density. In very thin films this density is low. As a result, when the vortices are set in motion, it is likely that some vortices are nucleated and others are depinned. On the contrary, thick films have a high pinning sites density and the vortices are set in motion by depinning only. Consistently, since the jump width is large, the vortex motion occurs as the motion of straight vortices in very thin films. In thick films the distance between pinning centers is short and the vortex motion occurs either by deformation of the vortex lines or by the motion of pancake vortices. As a result, very thin films can be driven in the flux flow regime with no thermal runaway in a large temperature range, but this is possible for thick films in the near vicinity of T_c only. Finally, our results are consistent with the suggestion that the cause of the high pinning sites density found in thick YBCO films is the stress relaxation occurring during film growth.

ACKNOWLEDGMENTS

We are grateful to Dr. C. Simon and Dr. C. Goupil from CRISMAT-ISMRA for very fruitful discussions. We thank M. Hanotel for her contribution to the photolithographic process and B. Pouderoux for the improvement of the measurements system.

APPENDIX: DEMAGNETIZING FIELD FACTOR FOR A THIN STRIP

In the framework of the critical state model,[22,26] the value of the screening sheet current along the edges of a superconducting strip is written as

$$I_{sc}^0 = \int_{-d/2}^{d/2} \left| J\left(\frac{w}{2}, z\right) \right| dz = \frac{B}{\mu_0} \sqrt{\pi w/\Lambda}, \tag{A1a}$$

with

$$\Lambda = \frac{2\lambda^2}{d}. \tag{A1b}$$

For a very thin strip we can write

$$\int_{-d/2}^{d/2} \left| J\left(\frac{w}{2}, z\right) \right| dz = J_{sc}^0 d, \tag{A2}$$

and we obtain

$$J_{sc}^0 = \frac{B}{\mu_0 \lambda} \sqrt{\pi w/2d}. \tag{A3}$$

Equation (A3) is similar to Eq. (2a) in the text, except for the term $\sqrt{\pi w/2d}$. This term is a demagnetizing field factor very similar to the expression derived by two-dimensional conformal mapping for objects infinite in the x direction by Provost, Paumier, and Fortini.[47]

*Also at CRISMAT-ISMRA, Cean, France.

[1] X. Xiaojun, F. Lan, W. Liangbin, Z. Yuheng, F. Jun, C. Xiaowen, L. Kebin, and S. Hisashi, Phys. Rev. B **59**, 608 (1999).
[2] H. C. Yang, L. M. Wang, and H. E. Horng, Phys. Rev. B **59**, 8956 (1999).
[3] O. Brunner, L. Antognazza, J. M. Triscone, L. Miéville, and O. Fischer, Phys. Rev. Lett. **67**, 1354 (1991).
[4] E. Zeldov, N. M. Amer, G. Koren, A. A. Gupta, M. W. McElfresh, and R. J. Gambino, Appl. Phys. Lett. **56**, 680 (1990).
[5] B. J. Jönsson, K. V. Rao, S. H. Yun, and U. O. Karlsson, Phys. Rev. B **58**, 5862 (1998).
[6] C. J. van der Beek, V. B. Geshkenbein, and V. M. Vinokur, Phys. Rev. B **48**, 3393 (1993).
[7] M. Zeisberger, Th. Klupsch, W. Michalke, and S. Linzen, in *Proceedings of EUCAS 95*, IOP Conf. Proc. No. 148 (Institute of Physics, London, 1995), p. 967.
[8] H. Obara, M. Andersson, L. Fabrega, P. Fivat, J. M. Triscone, M. Decroux, and O. Fischer, Phys. Rev. Lett. **74**, 3041 (1995).
[9] P. Bernstein, C. Picard, M. Pannetier, Ph. Lecoeur, J. F. Hamet, T. D. Doan, J. P. Contour, M. Drouet, and F. X. Regi, J. Appl. Phys. **82**, 5030 (1997).
[10] R. M. Schalk, G. Samadi Hosseinali, H. W. Weber, S. Proyer, P. Schwab, D. Bäuerle, and S. Gründorfer, Phys. Rev. B **49**, 3511 (1994).
[11] J. M. Triscone and O. Fischer, Rep. Prog. Phys. **60**, 1673 (1997).
[12] M. Ziese, P. Esquinazi, and H. F. Braun, Supercond. Sci. Technol. **7**, 869 (1994).
[13] J. Owliaei, S. Sridhar, and J. Talvacchio, Phys. Rev. Lett. **69**, 3366 (1992).
[14] M. Golosovsky, M. Tsindlekht, H. Chayet, and D. Davidov, Phys. Rev. B **50**, 470 (1994).
[15] A. M. Campbell, Cryogenics **30**, 809 (1990).
[16] W. S. Seow, R. A. Doyle, J. D. Johnson, D. Kumar, R. Somekh, D. J. C. Walker, and A. M. Campbell, Physica C **241**, 71 (1995).
[17] R. A. Doyle, A. M. Campbell, and R. Somekh, Phys. Rev. Lett. **71**, 4241 (1993).
[18] Y. Yokoyama, Y. Hasumi, H. Obara, Y. Suzuki, T. Katayama, S. Gotoh, and N. Koshizuka, Jpn. J. Appl. Phys., Part 2 **30**, L714 (1991).
[19] P. D. Grant, M. W. Denhoff, W. Xing, P. Brown, S. Govorkov, J. C. Irwin, B. Heinrich, H. Zhou, A. A. Fife, and A. R. Cragg, Physica C **229**, 289 (1994).
[20] H. Darhamaoui, J. Jung, J. Talvacchio, M. A.-K. Mohamed, and L. Friedrich, Phys. Rev. B **53**, 12 330 (1996).

[21] W. Xing, B. Heinrich, H. Zhou, A. A. Fife, and A. R. Cragg, J. Appl. Phys. **76**, 4244 (1994).
[22] E. H. Brandt and M. Indenbom, Phys. Rev. B **48**, 12 893 (1993).
[23] E. H. Brandt, Rep. Prog. Phys. **58**, 1465 (1995).
[24] C. P. Bean and J. D. Livingstone, Phys. Rev. Lett. **12**, 14 (1964).
[25] E. Zeldov, A. I. Larkin, V. B. Geshkenbein, M. Konczykowsky, D. Majer, B. Khaykovich, V. M. Vinokur, and H. Shtrikman, Phys. Rev. Lett. **73**, 1428 (1994).
[26] A. V. Kuznetsov, D. V. Eremenko, and V. N. Trofimov, Phys. Rev. B **59**, 1507 (1999).
[27] K. K. Likharev, Zh. Eksp. Teor. Fiz. **61**, 1700 (1971) [Sov. Phys. JETP **34**, 906 (1972)].
[28] I. Aranson, M. Gitterman, and B. Ya. Shapiro, Phys. Rev. B **51**, 3092 (1995).
[29] T. Van Duzer and C. W. Turner, *Principles of Superconductive Devices* (Elsevier, New York, 1981).
[30] M. E. Gaevski, A. V. Bobyl, D. V. Shantsev, Y. M. Galperin, T. H. Johansen, M. Baziljevich, H. Bratsberg, and S. F. Karmanenko, Phys. Rev. B **59**, 9655 (1999).
[31] P. W. Anderson and Y. B. Kim, Rev. Mod. Phys. **36**, 39 (1964).
[32] Ch. Goupil, T. Aouaroun, D. Thopart, J. F. Hamet, and Ch. Simon, Phys. Rev. B **54**, 15 525 (1996).
[33] E. H. Brandt, Phys. Rev. Lett. **69**, 1105 (1992).
[34] E. H. Brandt, Z. Phys. B: Condens. Matter **80**, 167 (1990).
[35] R. Desfeux, J. F. Hamet, B. Mercey, Ch. Simon, M. Hervieu, and B. Raveau, Physica C **221**, 205 (1994).
[36] Too few data were available in the case of microbridge S3 to obtain a reliable result.
[37] S. Revenaz, D. E. Oates, D. Labbé-Lavigne, G. Dresselhaus, and M. S. Dresslhaus, Phys. Rev. B **50**, 1178 (1994).
[38] N. Belk, D. E. Oates, D. A. Feld, G. Dresselhaus, and M. S. Dresselhaus, Phys. Rev. B **53**, 3459 (1996).
[39] N. Belk, D. E. Oates, D. A. Feld, G. Dresselhaus, and M. S. Dresselhaus, Phys. Rev. B **56**, 11 966 (1997).
[40] M. Pannetier, P. Bernstein, Ph. Lecoeur, O. Riou, T. D. Doan, J. F. Hamet, IEEE Trans. Appl. Supercond. **9**, 2635 (1999).
[41] B. A. Willemsen, J. S. Derov, and S. Sridhar, Phys. Rev. B **56**, 11 989 (1997).
[42] J. P. Contour, A. Défossez, D. Ravelosona, A. Abert, and P. Ziemann, Z. Phys. B: Condens. Matter **100**, 185 (1996).
[43] J. P. Contour, A. Abert, and A. Défossez, Proc. SPIE **2697**, 339 (1996).
[44] A. I. Larkin and Y. M. Ovchinnikov, J. Low Temp. Phys. **34**, 409 (1979).
[45] A. I. Larkin and Y. M. Ovchinnikov, J. Low Temp. Phys. **37**, 109 (1979).
[46] G. Blatter, M. V. Feigel'man, V. B. Geshkenbein, A. I. Larkin, and V. M. Vinokur, Rev. Mod. Phys. **66**, 1125 (1994).
[47] J. Provost, E. Paumier, and A. Fortini, J. Phys. F: Met. Phys. **4**, 439 (1974).